

This is the accepted manuscript made available via CHORUS. The article has been published as:

Cross section and double helicity asymmetry for η mesons
and their comparison to π^0 production in p+p collisions
at $\sqrt{s}=200$ GeV

A. Adare *et al.* (PHENIX Collaboration)

Phys. Rev. D **83**, 032001 — Published 1 February 2011

DOI: [10.1103/PhysRevD.83.032001](https://doi.org/10.1103/PhysRevD.83.032001)

Cross section and double helicity asymmetry for η mesons and their comparison to π^0 production in $p + p$ collisions at $\sqrt{s} = 200$ GeV

A. Adare,¹¹ S. Afanasiev,²⁵ C. Aidala,^{12,36} N.N. Ajitanand,⁵³ Y. Akiba,^{47,48} H. Al-Bataineh,⁴² J. Alexander,⁵³ K. Aoki,^{30,47} L. Aphecetche,⁵⁵ R. Armendariz,⁴² S.H. Aronson,⁶ J. Asai,^{47,48} E.T. Atomssa,³¹ R. Averbeck,⁵⁴ T.C. Awes,⁴³ B. Azmoun,⁶ V. Babintsev,²¹ M. Bai,⁵ G. Baksay,¹⁷ L. Baksay,¹⁷ A. Baldisseri,¹⁴ K.N. Barish,⁷ P.D. Barnes,³³ B. Bassalleck,⁴¹ A.T. Basye,¹ S. Bathe,⁷ S. Batsouli,⁴³ V. Baublis,⁴⁶ C. Baumann,³⁷ A. Bazilevsky,⁶ S. Belikov,^{6,*} R. Bennett,⁵⁴ A. Berdnikov,⁵⁰ Y. Berdnikov,⁵⁰ A.A. Bickley,¹¹ J.G. Boissevain,³³ H. Borel,¹⁴ K. Boyle,⁵⁴ M.L. Brooks,³³ H. Buesching,⁶ V. Bumazhnov,²¹ G. Bunce,^{6,48} S. Butsyk,^{33,54} C.M. Camacho,³³ S. Campbell,⁵⁴ B.S. Chang,⁶² W.C. Chang,² J.-L. Charvet,¹⁴ S. Chernichenko,²¹ J. Chiba,²⁶ C.Y. Chi,¹² M. Chiu,²² I.J. Choi,⁶² R.K. Choudhury,⁴ T. Chujo,^{58,59} P. Chung,⁵³ A. Churn,²¹ V. Cianciolo,⁴³ Z. Citron,⁵⁴ C.R. Cleven,¹⁹ B.A. Cole,¹² M.P. Comets,⁴⁴ P. Constantin,³³ M. Csanád,¹⁶ T. Csörgő,²⁷ T. Dahms,⁵⁴ S. Dairaku,^{30,47} K. Das,¹⁸ G. David,⁶ M.B. Deaton,¹ K. Dehmelt,¹⁷ H. Delagrange,⁵⁵ A. Denisov,²¹ D. d'Enterria,^{12,31} A. Deshpande,^{48,54} E.J. Desmond,⁶ O. Dietzsch,⁵¹ A. Dion,⁵⁴ M. Donadelli,⁵¹ O. Drapier,³¹ A. Drees,⁵⁴ K.A. Drees,⁵ A.K. Dubey,⁶¹ A. Durum,²¹ D. Dutta,⁴ V. Dzhordzhadze,⁷ Y.V. Efremenko,⁴³ J. Egdemir,⁵⁴ F. Ellinghaus,¹¹ W.S. Emam,⁷ T. Engelmores,¹² A. Enokizono,³² H. En'yo,^{47,48} S. Esumi,⁵⁸ K.O. Eyser,⁷ B. Fadern,³⁸ D.E. Fields,^{41,48} M. Finger, Jr.,^{8,25} M. Finger,^{8,25} F. Fleuret,³¹ S.L. Fokin,²⁹ Z. Fraenkel,^{61,*} J.E. Frantz,⁵⁴ A. Franz,⁶ A.D. Frawley,¹⁸ K. Fujiwara,⁴⁷ Y. Fukao,^{30,47} T. Fusayasu,⁴⁰ S. Gadrat,³⁴ I. Garishvili,⁵⁶ A. Glenn,¹¹ H. Gong,⁵⁴ M. Gonin,³¹ J. Gosset,¹⁴ Y. Goto,^{47,48} R. Granier de Cassagnac,³¹ N. Grau,^{12,24} S.V. Greene,⁵⁹ M. Grosse Perdekamp,^{22,48} T. Gunji,¹⁰ H.-Å. Gustafsson,^{35,*} T. Hachiya,²⁰ A. Hadj Henni,⁵⁵ C. Haegemann,⁴¹ J.S. Haggerty,⁶ H. Hamagaki,¹⁰ R. Han,⁴⁵ H. Harada,²⁰ E.P. Hartouni,³² K. Haruna,²⁰ E. Haslum,³⁵ R. Hayano,¹⁰ M. Heffner,³² T.K. Hemmick,⁵⁴ T. Hester,⁷ X. He,¹⁹ H. Hiejima,²² J.C. Hill,²⁴ R. Hobbs,⁴¹ M. Hohmann,¹⁷ W. Holzmann,⁵³ K. Homma,²⁰ B. Hong,²⁸ T. Horaguchi,^{10,47,57} D. Hornback,⁵⁶ S. Huang,⁵⁹ T. Ichihara,^{47,48} R. Ichimiya,⁴⁷ H. Inuma,^{30,47} Y. Ikeda,⁵⁸ K. Imai,^{30,47} J. Imrek,¹⁵ M. Inaba,⁵⁸ Y. Inoue,^{49,47} D. Isenhowe,¹ L. Isenhowe,¹ M. Ishihara,⁴⁷ T. Isobe,¹⁰ M. Issah,⁵³ A. Isupov,²⁵ D. Ivanischev,⁴⁶ B.V. Jacak,^{54,†} J. Jia,¹² J. Jin,¹² O. Jinnouchi,⁴⁸ B.M. Johnson,⁶ K.S. Joo,³⁹ D. Jouan,⁴⁴ F. Kajihara,¹⁰ S. Kametani,^{10,47,60} N. Kamihara,^{47,48} J. Kamin,⁵⁴ M. Kaneta,⁴⁸ J.H. Kang,⁶² H. Kanou,^{47,57} J. Kapustinsky,³³ D. Kawał,^{36,48} A.V. Kazantsev,²⁹ T. Kempel,²⁴ A. Khanzadeev,⁴⁶ K.M. Kijima,²⁰ J. Kikuchi,⁶⁰ B.I. Kim,²⁸ D.H. Kim,³⁹ D.J. Kim,⁶² E. Kim,⁵² S.H. Kim,⁶² E. Kinney,¹¹ K. Kiriluk,¹¹ Á. Kiss,¹⁶ E. Kistenev,⁶ A. Kiyomichi,⁴⁷ J. Klay,³² C. Klein-Boesing,³⁷ L. Kochenda,⁴⁶ V. Kochetkov,²¹ B. Komkov,⁴⁶ M. Konno,⁵⁸ J. Koster,²² D. Korchetkov,⁷ A. Kozlov,⁶¹ A. Král,¹³ A. Kravitz,¹² J. Kubart,^{8,23} G.J. Kunde,³³ N. Kurihara,¹⁰ K. Kurita,^{49,47} M. Kurosawa,⁴⁷ M.J. Kweon,²⁸ Y. Kwon,^{56,62} G.S. Kyle,⁴² R. Lacey,⁵³ Y.S. Lai,¹² J.G. Lajoie,²⁴ D. Layton,²² A. Lebedev,²⁴ D.M. Lee,³³ K.B. Lee,²⁸ M.K. Lee,⁶² T. Lee,⁵² M.J. Leitch,³³ M.A.L. Leite,⁵¹ B. Lenzi,⁵¹ P. Liebing,⁴⁸ T. Liška,¹³ A. Litvinenko,²⁵ H. Liu,⁴² M.X. Liu,³³ X. Li,⁹ B. Love,⁵⁹ D. Lynch,⁶ C.F. Maguire,⁵⁹ Y.I. Makdisi,⁵ A. Malakhov,²⁵ M.D. Malik,⁴¹ V.I. Manko,²⁹ E. Mannel,¹² Y. Mao,^{45,47} L. Mašek,^{8,23} H. Masui,⁵⁸ F. Matathias,¹² M. McCumber,⁵⁴ P.L. McGaughey,³³ N. Means,⁵⁴ B. Meredith,²² Y. Miake,⁵⁸ P. Mikeš,^{8,23} K. Miki,⁵⁸ T.E. Miller,⁵⁹ A. Milov,^{6,54} S. Mioduszewski,⁶ M. Mishra,³ J.T. Mitchell,⁶ M. Mitrovski,⁵³ A.K. Mohanty,⁴ Y. Morino,¹⁰ A. Morreale,⁷ D.P. Morrison,⁶ T.V. Moukhanova,²⁹ D. Mukhopadhyay,⁵⁹ J. Murata,^{49,47} S. Nagamiya,²⁶ Y. Nagata,⁵⁸ J.L. Nagle,¹¹ M. Naglis,⁶¹ M.I. Nagy,¹⁶ I. Nakagawa,^{47,48} Y. Nakamiya,²⁰ T. Nakamura,²⁰ K. Nakano,^{47,57} J. Newby,³² M. Nguyen,⁵⁴ T. Niita,⁵⁸ B.E. Norman,³³ R. Nouicer,⁶ A.S. Nyanin,²⁹ E. O'Brien,⁶ S.X. Oda,¹⁰ C.A. Ogilvie,²⁴ H. Ohnishi,⁴⁷ K. Okada,⁴⁸ M. Oka,⁵⁸ O.O. Omiwade,¹ Y. Onuki,⁴⁷ A. Oskarsson,³⁵ M. Ouchida,²⁰ K. Ozawa,¹⁰ R. Pak,⁶ D. Pal,⁵⁹ A.P.T. Palounek,³³ V. Pantuev,⁵⁴ V. Papavassiliou,⁴² J. Park,⁵² W.J. Park,²⁸ S.F. Pate,⁴² H. Pei,²⁴ J.-C. Peng,²² H. Pereira,¹⁴ V. Peresedov,²⁵ D.Yu. Peressounko,²⁹ C. Pinkenburg,⁶ M.L. Purschke,⁶ A.K. Purwar,³³ H. Qu,¹⁹ J. Rak,⁴¹ A. Rakotozafindrabe,³¹ I. Ravinovich,⁶¹ K.F. Read,^{43,56} S. Rembeczki,¹⁷ M. Reuter,⁵⁴ K. Reygers,³⁷ V. Riabov,⁴⁶ Y. Riabov,⁴⁶ D. Roach,⁵⁹ G. Roche,³⁴ S.D. Rolnick,⁷ A. Romana,^{31,*} M. Rosati,²⁴ S.S.E. Rosendahl,³⁵ P. Rosnet,³⁴ P. Rukoyatkin,²⁵ P. Ružička,²³ V.L. Rykov,⁴⁷ B. Sahlmueller,³⁷ N. Saito,^{30,47,48} T. Sakaguchi,⁶ S. Sakai,⁵⁸ K. Sakashita,^{47,57} H. Sakata,²⁰ V. Samsonov,⁴⁶ S. Sato,²⁶ T. Sato,⁵⁸ S. Sawada,²⁶ K. Sedgwick,⁷ J. Seele,¹¹ R. Seidl,²² A.Yu. Semenov,²⁴ V. Semenov,²¹ R. Seto,⁷ D. Sharma,⁶¹ I. Shein,²¹ A. Shevel,^{46,53} T.-A. Shibata,^{47,57} K. Shigaki,²⁰ M. Shimomura,⁵⁸ K. Shoji,^{30,47} P. Shukla,⁴ A. Sickles,^{6,54} C.L. Silva,⁵¹ D. Silvermyr,⁴³ C. Silvestre,¹⁴ K.S. Sim,²⁸ B.K. Singh,³ C.P. Singh,³ V. Singh,³ S. Skutnick,²⁴ M. Slunečka,^{8,25} A. Soldatov,²¹ R.A. Soltz,³² W.E. Sondheim,³³ S.P. Sorensen,⁵⁶ I.V. Sourikova,⁶ F. Staley,¹⁴ P.W. Stankus,⁴³ E. Stenlund,³⁵ M. Stepanov,⁴² A. Ster,²⁷ S.P. Stoll,⁶ T. Sugitate,²⁰ C. Suire,⁴⁴ A. Sukhanov,⁶ J. Sziklai,²⁷ T. Tabaru,⁴⁸ S. Takagi,⁵⁸ E.M. Takagui,⁵¹ A. Taketani,^{47,48} R. Tanabe,⁵⁸ Y. Tanaka,⁴⁰

S. Taneja,⁵⁴ K. Tanida,^{47,48,52} M.J. Tannenbaum,⁶ A. Taranenko,⁵³ P. Tarján,¹⁵ H. Themann,⁵⁴ T.L. Thomas,⁴¹
M. Togawa,^{30,47} A. Toia,⁵⁴ J. Tojo,⁴⁷ L. Tomášek,²³ Y. Tomita,⁵⁸ H. Torii,^{20,47} R.S. Towell,¹ V-N. Tram,³¹
I. Tserruya,⁶¹ Y. Tsuchimoto,²⁰ C. Vale,²⁴ H. Valle,⁵⁹ H.W. van Hecke,³³ A. Veicht,²² J. Velkovska,⁵⁹ R. Vértesi,¹⁵
A.A. Vinogradov,²⁹ M. Virius,¹³ V. Vrba,²³ E. Vznuzdaev,⁴⁶ M. Wagner,^{30,47} D. Walker,⁵⁴ X.R. Wang,⁴²
Y. Watanabe,^{47,48} F. Wei,²⁴ J. Wessels,³⁷ S.N. White,⁶ D. Winter,¹² C.L. Woody,⁶ M. Wysocki,¹¹ W. Xie,⁴⁸
Y.L. Yamaguchi,⁶⁰ K. Yamaura,²⁰ R. Yang,²² A. Yanovich,²¹ Z. Yasin,⁷ J. Ying,¹⁹ S. Yokkaichi,^{47,48} G.R. Young,⁴³
I. Younus,⁴¹ I.E. Yushmanov,²⁹ W.A. Zajc,¹² O. Zaudtke,³⁷ C. Zhang,⁴³ S. Zhou,⁹ J. Zimányi,^{27,*} and L. Zolin²⁵

(PHENIX Collaboration)

¹Abilene Christian University, Abilene, Texas 79699, USA

²Institute of Physics, Academia Sinica, Taipei 11529, Taiwan

³Department of Physics, Banaras Hindu University, Varanasi 221005, India

⁴Bhabha Atomic Research Centre, Bombay 400 085, India

⁵Collider-Accelerator Department, Brookhaven National Laboratory, Upton, New York 11973-5000, USA

⁶Physics Department, Brookhaven National Laboratory, Upton, New York 11973-5000, USA

⁷University of California - Riverside, Riverside, California 92521, USA

⁸Charles University, Ovocný trh 5, Praha 1, 116 36, Prague, Czech Republic

⁹China Institute of Atomic Energy (CIAE), Beijing, People's Republic of China

¹⁰Center for Nuclear Study, Graduate School of Science, University of Tokyo, 7-3-1 Hongo, Bunkyo, Tokyo 113-0033, Japan

¹¹University of Colorado, Boulder, Colorado 80309, USA

¹²Columbia University, New York, New York 10027 and Nevis Laboratories, Irvington, New York 10533, USA

¹³Czech Technical University, Zikova 4, 166 36 Prague 6, Czech Republic

¹⁴Dapnia, CEA Saclay, F-91191, Gif-sur-Yvette, France

¹⁵Debrecen University, H-4010 Debrecen, Egyetem tér 1, Hungary

¹⁶ELTE, Eötvös Loránd University, H - 1117 Budapest, Pázmány P. s. 1/A, Hungary

¹⁷Florida Institute of Technology, Melbourne, Florida 32901, USA

¹⁸Florida State University, Tallahassee, Florida 32306, USA

¹⁹Georgia State University, Atlanta, Georgia 30303, USA

²⁰Hiroshima University, Kagamiyama, Higashi-Hiroshima 739-8526, Japan

²¹IHEP Protvino, State Research Center of Russian Federation, Institute for High Energy Physics, Protvino, 142281, Russia

²²University of Illinois at Urbana-Champaign, Urbana, Illinois 61801, USA

²³Institute of Physics, Academy of Sciences of the Czech Republic, Na Slovance 2, 182 21 Prague 8, Czech Republic

²⁴Iowa State University, Ames, Iowa 50011, USA

²⁵Joint Institute for Nuclear Research, 141980 Dubna, Moscow Region, Russia

²⁶KEK, High Energy Accelerator Research Organization, Tsukuba, Ibaraki 305-0801, Japan

²⁷KFKI Research Institute for Particle and Nuclear Physics of the Hungarian Academy of Sciences (MTA KFKI RMKI), H-1525 Budapest 114, POBox 49, Budapest, Hungary

²⁸Korea University, Seoul, 136-701, Korea

²⁹Russian Research Center "Kurchatov Institute", Moscow, Russia

³⁰Kyoto University, Kyoto 606-8502, Japan

³¹Laboratoire Leprince-Ringuet, Ecole Polytechnique, CNRS-IN2P3, Route de Saclay, F-91128, Palaiseau, France

³²Lawrence Livermore National Laboratory, Livermore, California 94550, USA

³³Los Alamos National Laboratory, Los Alamos, New Mexico 87545, USA

³⁴LPC, Université Blaise Pascal, CNRS-IN2P3, Clermont-Fd, 63177 Aubiere Cedex, France

³⁵Department of Physics, Lund University, Box 118, SE-221 00 Lund, Sweden

³⁶Department of Physics, University of Massachusetts, Amherst, Massachusetts 01003-9337, USA

³⁷Institut für Kernphysik, University of Muenster, D-48149 Muenster, Germany

³⁸Muhlenberg College, Allentown, Pennsylvania 18104-5586, USA

³⁹Myongji University, Yongin, Kyonggido 449-728, Korea

⁴⁰Nagasaki Institute of Applied Science, Nagasaki-shi, Nagasaki 851-0193, Japan

⁴¹University of New Mexico, Albuquerque, New Mexico 87131, USA

⁴²New Mexico State University, Las Cruces, New Mexico 88003, USA

⁴³Oak Ridge National Laboratory, Oak Ridge, Tennessee 37831, USA

⁴⁴IPN-Orsay, Université Paris Sud, CNRS-IN2P3, BP1, F-91406, Orsay, France

⁴⁵Peking University, Beijing, People's Republic of China

⁴⁶PNPI, Petersburg Nuclear Physics Institute, Gatchina, Leningrad region, 188300, Russia

⁴⁷RIKEN Nishina Center for Accelerator-Based Science, Wako, Saitama 351-0198, Japan

⁴⁸RIKEN BNL Research Center, Brookhaven National Laboratory, Upton, New York 11973-5000, USA

⁴⁹Physics Department, Rikkyo University, 3-34-1 Nishi-Ikebukuro, Toshima, Tokyo 171-8501, Japan

⁵⁰Saint Petersburg State Polytechnic University, St. Petersburg, Russia

⁵¹Universidade de São Paulo, Instituto de Física, Caixa Postal 66318, São Paulo CEP05315-970, Brazil

⁵²Seoul National University, Seoul, Korea

⁵³Chemistry Department, Stony Brook University, SUNY, Stony Brook, New York 11794-3400, USA

⁵⁴*Department of Physics and Astronomy, Stony Brook University, SUNY, Stony Brook, New York 11794-3400, USA*

⁵⁵*SUBATECH (Ecole des Mines de Nantes, CNRS-IN2P3, Université de Nantes) BP 20722 - 44307, Nantes, France*

⁵⁶*University of Tennessee, Knoxville, Tennessee 37996, USA*

⁵⁷*Department of Physics, Tokyo Institute of Technology, Oh-okayama, Meguro, Tokyo 152-8551, Japan*

⁵⁸*Institute of Physics, University of Tsukuba, Tsukuba, Ibaraki 305, Japan*

⁵⁹*Vanderbilt University, Nashville, Tennessee 37235, USA*

⁶⁰*Waseda University, Advanced Research Institute for Science and Engineering, 17 Kikui-cho, Shinjuku-ku, Tokyo 162-0044, Japan*

⁶¹*Weizmann Institute, Rehovot 76100, Israel*

⁶²*Yonsei University, IPAP, Seoul 120-749, Korea*

Measurements of double helicity asymmetries in inclusive hadron production in polarized $p + p$ collisions are sensitive to helicity-dependent parton distribution functions, in particular to the gluon helicity distribution, Δg . This study focuses on the extraction of the double helicity asymmetry in η production ($\vec{p} + \vec{p} \rightarrow \eta + X$), the η cross section and the η/π^0 cross section ratio. The cross section and ratio measurements provide essential input for the extraction of fragmentation functions that are needed to access the helicity-dependent parton distribution functions.

PACS numbers: 13.85.Ni, 13.88.+e, 14.20.Dh

I. INTRODUCTION

Until recently, the knowledge about helicity-dependent parton distribution functions (PDFs) in the nucleon mainly came from next-to-leading order (NLO) QCD fits (see, e.g., [1]) to the helicity-dependent structure function g_1 , as measured in fixed-target polarized inclusive deep-inelastic scattering (DIS) experiments (see, e.g., [2, 3]). The resulting helicity-dependent PDF for the gluon has rather large uncertainties due to the fact that the exchanged virtual photon does not couple directly, i.e., at leading order, to the gluon, and that an indirect way of accessing it via NLO fits to g_1 suffers from the limited kinematic reach of the fixed target experiments. Accessing the helicity-dependent gluon PDF via the so-called photon-gluon-fusion process in semi-inclusive DIS has not yet resulted in better constraints, see Ref. [4, 5] and references therein for details. Thus, additional data from polarized $p + p$ scattering, in which longitudinally polarized gluons are directly probed via scattering off longitudinally polarized gluons or quarks, has the potential to reduce the uncertainties in the helicity-dependent gluon PDF. This has been demonstrated in a global NLO fit [6] using, for the first time, the available inclusive and semi-inclusive polarized DIS data together with first results from polarized $p + p$ scattering at the Relativistic Heavy Ion Collider (RHIC). The results included were the double helicity asymmetries in inclusive π^0 [7–9] and jet [10] production from the PHENIX and STAR experiments, respectively.

The double helicity asymmetry in inclusive hadron production is given as

$$A_{LL} = \frac{\sigma^{++} - \sigma^{+-}}{\sigma^{++} + \sigma^{+-}} \quad (1)$$

$$= \frac{\sum_{abc} \Delta f_a \otimes \Delta f_b \otimes \Delta \hat{\sigma}^{ab \rightarrow cX'} \otimes D_c^h}{2\sigma},$$

where the cross section σ^{++} (σ^{+-}) describes the reaction where both protons have the same (opposite) helicity. The helicity-independent cross section is defined as $\sigma = (\sigma^{++} + \sigma^{+-})/2$. The helicity-dependent decomposition of the numerator is given on the right-hand side of Eq. 1, where Δf_a , Δf_b represent the helicity-dependent PDFs for quarks or gluons, and $\Delta \hat{\sigma}$ are the helicity-dependent hard scattering cross sections calculable in perturbative QCD (pQCD). The kinematic dependences of these terms are omitted for simplicity. At leading order (LO) the fragmentation functions D_c^h can be interpreted as the probability for a certain parton c to fragment into a certain hadron h and thus they are not needed in the case of jet and direct photon production. In current global fits of parton helicity distributions, the fragmentation functions are assumed to be spin independent.

This study focuses on the midrapidity cross section and double helicity asymmetry in inclusive η production ($\vec{p} + \vec{p} \rightarrow \eta + X$) as a function of transverse momentum (p_T) and the η/π^0 cross section ratio at $\sqrt{s} = 200$ GeV measured at

*Deceased

†PHENIX Spokesperson: jacak@skipper.physics.sunysb.edu

the PHENIX experiment at RHIC. The measurement of the η double helicity asymmetry adds independent data with different systematics to the present set of polarized data available to PDF fits. Even when compared to a closely related data set, e.g., the PHENIX π^0 data on double helicity asymmetries, the difference in the fragmentation functions can lead to a different sensitivity to certain helicity-dependent PDFs. In contrast to the π^0 , the experimental data available to extract η fragmentation functions is rather limited. The existing η cross section measurements from $e^+ + e^-$ collider data can constrain the quark fragmentation functions to some degree, but the extraction of gluon fragmentation functions requires either rather precise $e^+ + e^-$ data taken in a wide range of center of mass energies, or cross section measurements from processes where gluons are directly involved, e.g., $p + p$ scattering. Therefore, the data on cross sections and cross section ratios presented here serve as important input for the extraction of fragmentation functions, in particular as the measurement has been performed over a wide range of p_T .

II. EXTRACTION OF η AND π^0 YIELDS

The η (π^0) meson is reconstructed through its main decay channel, η (π^0) $\rightarrow \gamma\gamma$, with a branching ratio (BR) of about 39% (99%) [11]. The data were taken at the PHENIX [12] experiment in 2005 and 2006. After data quality and vertex cuts, 2.5 pb^{-1} from the 2005 data and 6.5 pb^{-1} from the 2006 data are used for the analysis. The data sets from both years are used for the extraction of the statistics-limited double helicity asymmetry in η production while only the larger data set from 2006 is used for the extraction of the predominantly systematics-limited cross section measurements. Note that the analysis described in the following, including all cuts, is done in the exact same way for the η and the π^0 meson in order to minimize the systematic uncertainties on the η/π^0 cross section ratio presented below.

Two data sets have been analyzed, collected by requiring two different trigger selections. The minimum bias (MB) trigger requires coincident signals in two beam-beam counters (BBCs) [13], which are arrays of quartz-radiator Čerenkov counters providing full azimuthal coverage at pseudorapidities of $3.0 < |\eta| < 3.9$. Based on the timing of the signals from the two BBCs, the event vertex is reconstructed and required to be within 30 cm of the nominal interaction point. In addition to the MB trigger, the high- p_T triggered data set requires an energy deposition larger than approximately 1.4 GeV in an area of 4×4 towers in the electromagnetic calorimeter (EMCal) [14].

The EMCal is the primary detector used in this analysis, located at a radial distance of about 5 m from the beam pipe. It covers the pseudo-rapidity range $|\eta| < 0.35$ and has an azimuthal acceptance of $\Delta\phi = \pi$. The EMCal comprises eight sectors, six of which are composed of a total of 15552 lead-scintillator (PbSc) sandwich towers ($5.5 \text{ cm} \times 5.5 \text{ cm} \times 37.5 \text{ cm}$), and two sectors of lead-glass (PbGl) Čerenkov calorimeters, consisting of a total of 9216 towers ($4 \text{ cm} \times 4 \text{ cm} \times 40 \text{ cm}$). For the cross section measurements only the PbSc was used.

A cluster in the EMCal is assumed to originate from a photon if the following criteria are met. First, since showers in the EMCal are not confined to a single tower, a shower profile analysis can be used to reject hadrons, which usually produce broader showers than photons. Since hadrons are slower than photons, an additional time of flight cut is used for photon identification. Furthermore, the cluster must not be associated with a hit from a charged particle in the Pad Chamber (PC3) just in front of the EMCal; an exception is made if the hit position in the EMCal and in the PC3 are aligned in such a way that the particle could have come from the vertex on a straight line, i.e., it was not bent in the central magnetic field. In this case, the cluster is accepted as a photon candidate since it is likely that the original photon converted into an e^+e^- pair before the PC3 but outside the magnetic field. The latter two selection cuts are used in the analysis of the double helicity asymmetry but not in the extraction of the cross sections, leading to a smaller signal to background ratio in the cross section measurements. In order to exclude clusters with potentially incorrectly reconstructed energies due to leakage effects, the tower with the largest energy deposition in a cluster must not be in the outermost two columns or rows of an EMCal sector. In addition, there must not be a noisy or dead tower in the eight towers surrounding the central one.

Using all possible pairs of photon candidates, the two-photon invariant mass spectrum is calculated. An upper limit of 0.7 is placed on the energy asymmetry, $|E_1 - E_2|/(E_1 + E_2)$, of the two cluster energies, E_1 and E_2 , in order to reduce the combinatorial background due to numerous low-energy background clusters. It is also checked that either of the two clusters coincides with an area in the EMCal that caused a high- p_T trigger. Finally, the p_T of the diphoton is required to be larger than 2 GeV/ c . At smaller p_T , the uncertainties in the cross section extraction become too large due to large backgrounds and limited acceptance.

The η and π^0 cross sections and the η double helicity asymmetry are extracted in bins of p_T . Using the selection cuts for the cross section extraction on the high- p_T triggered data set, the resulting invariant mass distributions in the vicinity of the η peak are shown in Fig. 1 for three different bins of p_T . For bins at small p_T , the signal extraction is based on fits to the invariant mass distributions using a Gaussian for the signal plus a second-order polynomial for the background that describe the vicinity of the η and π^0 peaks very well. For $p_T \gtrsim 10 \text{ GeV}/c$ the signal extraction based on fits becomes unreliable as limited statistics leads to large fluctuations in the fit results for the mean and

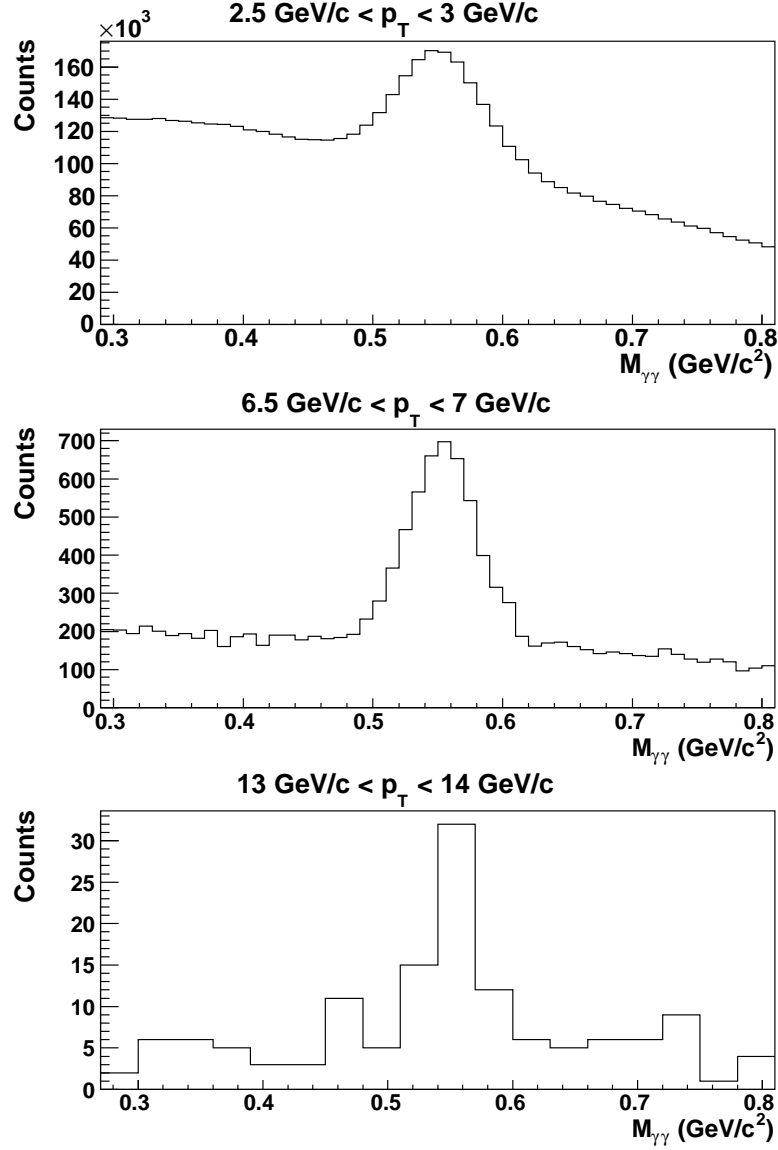


FIG. 1: Invariant mass distributions in the vicinity of the η peak for the high- p_T triggered data set and for three different bins of p_T . The selection cuts for the cross section extraction are used.

width of the peaks. Therefore, the mean and width are taken from a Monte-Carlo simulation, which describes the mean and width of the η and π^0 peaks as a function of p_T very well for bins in the mid- p_T range between 3 GeV/c and 10 GeV/c , giving confidence in using them for the bins above. This is demonstrated in Fig. 2 for the case of η production. The small discrepancies at $p_T < 3 \text{ GeV}/c$ are due to the large background underneath the peak, as can be seen in the top panel of Fig. 1, which is not modeled in the MC. Thus, above $p_T = 3 \text{ GeV}/c$ the number of background counts under the signal peak can be estimated by using the number of counts in the sidebands. The sidebands are on both sides of the mean of the peak, between 4 and 7 (4 and 6) times the Gaussian width of the peak for the cross section (double helicity asymmetry) analysis. However, the exact position and width of the sidebands are varied and possible effects are taken into account in the systematic uncertainty. In the mid- p_T range between 3 GeV/c and 10 GeV/c , where statistics is sufficient for the fit results to be stable and the background in the vicinity of the peaks is approximately linear so that the sideband subtraction is applicable, both methods agree as expected.

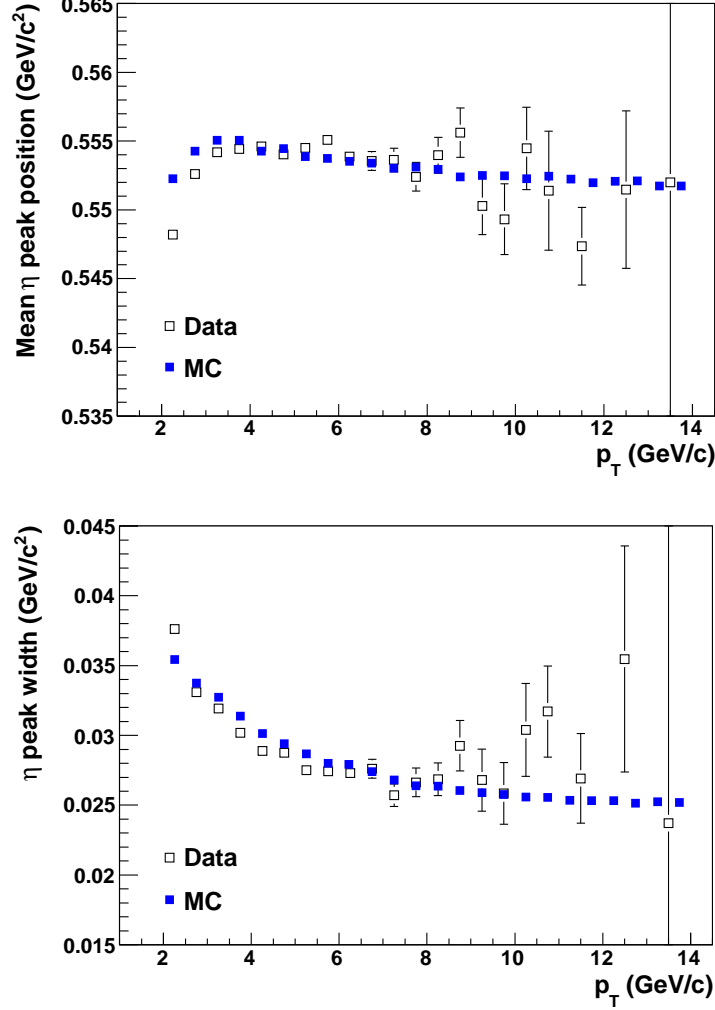


FIG. 2: Mean and width of the η peaks as a function of p_T for the high- p_T triggered data set and the MC. The selection cuts for the cross section extraction are used.

III. THE η CROSS SECTION AND η/π^0 CROSS SECTION RATIO

The η and π^0 meson cross sections are calculated from

$$E \frac{d^3\sigma}{d^3p} = \frac{1}{2\pi p_T} \frac{1}{BR} \frac{1}{\mathcal{L}} \frac{1}{A \epsilon_{\text{trig}} \epsilon_{\text{rec}}} \frac{N(\Delta p_T, \Delta y)}{\Delta p_T \Delta y}, \quad (2)$$

where \mathcal{L} denotes the integrated luminosity, A the acceptance, ϵ_{trig} the trigger efficiency, ϵ_{rec} the reconstruction efficiency, and N the number of reconstructed mesons.

The luminosity is calculated from the number of MB events divided by the cross section for events selected by the MB trigger. For the latter, a value of 23.0 mb with a systematic uncertainty of 9.7% has been derived from Vernier scan results [15] and an extrapolation for subsequent years. The acceptance is calculated from a Monte-Carlo simulation using, as an input, the map of noisy and dead cells also used in the data analysis. The systematic uncertainty on the acceptance calculation is 3.6% (3%) for the η (π^0) meson. The trigger efficiency for the MB data is given by the MB trigger efficiency for η and π^0 production. The trigger efficiency for the high- p_T triggered data set is given by the MB trigger efficiency times the efficiency of the high- p_T trigger. The MB (high- p_T) trigger efficiency is determined by the ratio of the number of reconstructed π^0 or η mesons in a high- p_T (MB) triggered sample in coincidence with the MB (high- p_T) trigger divided by the number of reconstructed π^0 or η events without the coincidence. The MB trigger efficiency is 0.78 for both π^0 and η mesons over the whole range of p_T considered, with a systematic uncertainty of

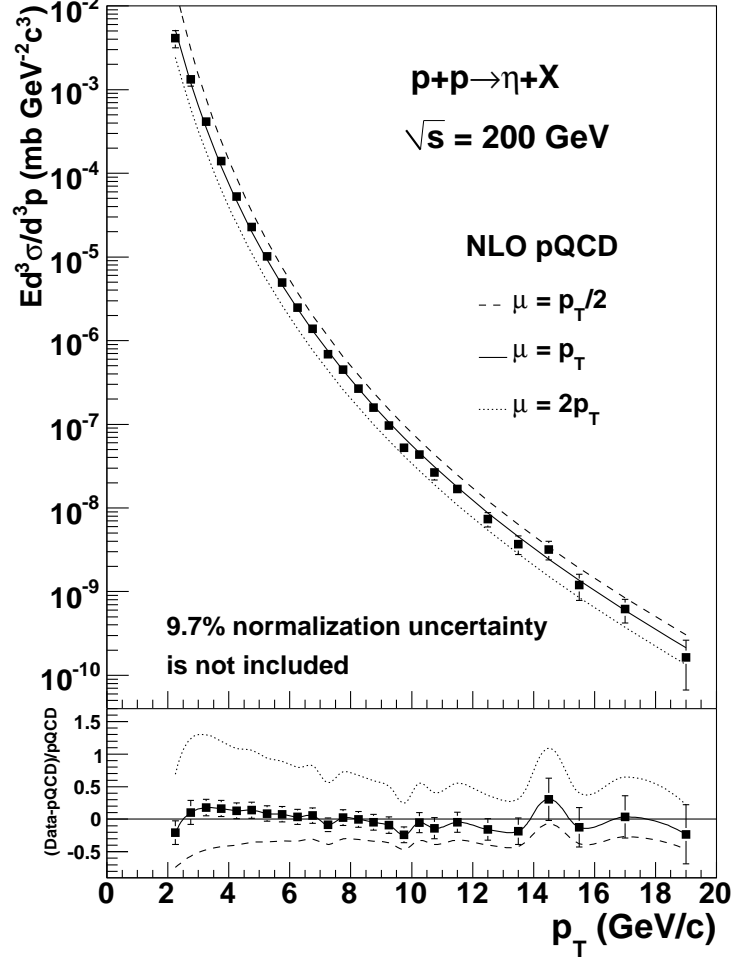


FIG. 3: Cross section for midrapidity inclusive η production at $\sqrt{s} = 200$ GeV as a function of p_T and its comparison to NLO pQCD calculations at three different scales μ . The error bars shown are the statistical and systematic uncertainties added in quadrature. Not included is the overall normalization uncertainty of 9.7%. Note that the fragmentation functions used in the calculations are partially constrained by this data. See text for details.

3%. The high- p_T trigger efficiency reaches a plateau at a level of 0.90 for $p_T > 4.5$ GeV/ c and is also very similar for both mesons. Due to the fact that the turn-on curve of the high p_T trigger is very steep and reaches an efficiency of about 0.80 in the $3 < p_T < 3.5$ GeV/ c bin, the efficiency for $p_T < 3$ GeV/ c has a large systematic uncertainty. Therefore, the cross section calculation is based on the smaller MB triggered data set for $p_T < 3$ GeV/ c and on the high- p_T triggered data set for larger transverse momenta. The reconstruction efficiency accounts for loss of photons due to conversion ($6\% \pm 2\%$) and due to the cut on the shower shape discussed above ($4\% \pm 2\%$). In the case of π^0 production, merging of the two decay photons into a single cluster is considered for $p_T > 10$ GeV/ c .

The η cross section as a function of p_T between 2 and 20 GeV/ c is shown in Fig. 3 and tabulated in Table I. Note that a bin-shift correction is applied in order to be able to plot each data point at the center of each given p_T bin, which, due to the exponentially falling spectrum, does not represent the true physical value of the yield in that bin [16]. This in particular facilitates the calculation of the η/π^0 cross section ratio.

The η cross section is consistent with an earlier PHENIX measurement [17] covering a smaller range in p_T from 2.5 to 12 GeV/ c . The error bars shown in Fig. 3 are the statistical and systematic uncertainties added in quadrature. Not included is an overall normalization uncertainty of 9.7% due to the uncertainty in the luminosity measurement. The other dominant systematic uncertainties are an approximately p_T -independent uncertainty of about 8% due to the uncertainty on the global energy scale of 1.2%, possible nonlinearities in the energy scale affecting mainly points with $p_T > 10$ GeV/ c , and uncertainties from the signal extraction affecting principally the two lowest p_T points, which have

TABLE I: Measured η cross sections vs p_T for the 2006 data set with statistical and systematic (type- B_1 and type- B_2) uncertainties. There is an additional normalization uncertainty of 9.7% (type- C).

p_T (GeV/c)	$E \frac{d^3\sigma}{dp^3}$ (mb GeV $^{-2}$ c 3)	stat	type- B_1	type- B_2
2.25	4.12×10^{-03}	0.22×10^{-03}	0.86×10^{-03}	0.32×10^{-03}
2.75	1.33×10^{-03}	0.07×10^{-03}	0.19×10^{-03}	0.10×10^{-03}
3.25	4.14×10^{-04}	0.02×10^{-04}	0.17×10^{-04}	0.41×10^{-04}
3.75	1.40×10^{-04}	0.01×10^{-04}	0.06×10^{-04}	0.14×10^{-04}
4.25	5.28×10^{-05}	0.04×10^{-05}	0.21×10^{-05}	0.53×10^{-05}
4.75	2.28×10^{-05}	0.02×10^{-05}	0.09×10^{-05}	0.23×10^{-05}
5.25	1.01×10^{-05}	0.01×10^{-05}	0.04×10^{-05}	0.10×10^{-05}
5.75	4.95×10^{-06}	0.08×10^{-06}	0.20×10^{-06}	0.50×10^{-06}
6.25	2.48×10^{-06}	0.05×10^{-06}	0.10×10^{-06}	0.25×10^{-06}
6.75	1.39×10^{-06}	0.04×10^{-06}	0.06×10^{-06}	0.14×10^{-06}
7.25	6.87×10^{-07}	0.26×10^{-07}	0.28×10^{-07}	0.71×10^{-07}
7.75	4.50×10^{-07}	0.19×10^{-07}	0.18×10^{-07}	0.46×10^{-07}
8.25	2.67×10^{-07}	0.14×10^{-07}	0.11×10^{-07}	0.28×10^{-07}
8.75	1.59×10^{-07}	0.10×10^{-07}	0.06×10^{-07}	0.16×10^{-07}
9.25	9.63×10^{-08}	0.78×10^{-08}	0.39×10^{-08}	1.03×10^{-08}
9.75	5.24×10^{-08}	0.58×10^{-08}	0.21×10^{-08}	0.56×10^{-08}
10.25	4.33×10^{-08}	0.48×10^{-08}	0.17×10^{-08}	0.48×10^{-08}
10.75	2.66×10^{-08}	0.39×10^{-08}	0.11×10^{-08}	0.30×10^{-08}
11.5	1.68×10^{-08}	0.19×10^{-08}	0.07×10^{-08}	0.19×10^{-08}
12.5	7.37×10^{-09}	1.14×10^{-09}	0.30×10^{-09}	0.86×10^{-09}
13.5	3.70×10^{-09}	0.79×10^{-09}	0.15×10^{-09}	0.45×10^{-09}
14.5	3.19×10^{-09}	0.67×10^{-09}	0.13×10^{-09}	0.41×10^{-09}
15.5	1.20×10^{-09}	0.38×10^{-09}	0.05×10^{-09}	0.15×10^{-09}
17	6.17×10^{-10}	1.74×10^{-10}	0.25×10^{-10}	0.83×10^{-10}
19	1.64×10^{-10}	0.95×10^{-10}	0.07×10^{-10}	0.22×10^{-10}

a large background underneath the η peak. The systematic uncertainties are subdivided into uncertainties that are uncorrelated between p_T bins (type- A), correlated between p_T bins (type- B), and overall normalization uncertainties (type- C). As described above, the peak extraction is based on different methods depending on p_T . Thus, the p_T bins in certain regions are correlated, but there is no full correlation over the whole range. Such kind of uncertainties are sub-categorized as type- B_1 , in order to distinguish from those correlated over all p_T bins (type- B_2). All other uncertainties, except the one from the luminosity measurement (type- C), are assumed to be in this category.

The η cross section from $p + p$ scattering presented here, together with the above mentioned earlier PHENIX data [17], and various η cross section measurements from $e^+ + e^-$ scattering have been used in a global fit to extract new fragmentation functions for η production at NLO [18]. The wide p_T range of this measurement, as compared to the earlier PHENIX measurement, which covers a range in p_T from 2.5 to 12 GeV/c, is important, because it allows for a much more stringent constraint on the η fragmentation function, as can be seen in Figs. 6 and 8 of Ref. [18].

Earlier determinations of η fragmentation functions based on SU(3) model estimates at LO and normalizations taken from a Monte Carlo event generator at NLO are described in Refs. [19, 20] and Ref. [21], respectively. Due to the absence of data on semi-inclusive η production the fragmentation functions can only be extracted separately for each quark flavor with additional assumptions. The assumption that all light quark fragmentation functions are the same, i.e., $D_u^\eta = D_d^\eta = D_s^\eta = D_{\bar{u}}^\eta = D_{\bar{d}}^\eta = D_{\bar{s}}^\eta$, has been used in Ref. [18].

Using these new fragmentation functions and the CTEQ6M [22] PDFs as an input to the NLO code of Ref. [23], pQCD calculations at three different scales μ are carried out. Here, μ represents the factorization, renormalization and fragmentation scales, i.e., the three scales are set equal in each separate calculation. With these new fragmentation functions, for which the present data constitute nearly 20% of the input experimental data points, the cross section is described well.

The contributions of the various scattering subprocesses, gluon-gluon (gg), quark-gluon (qg), and quark-quark

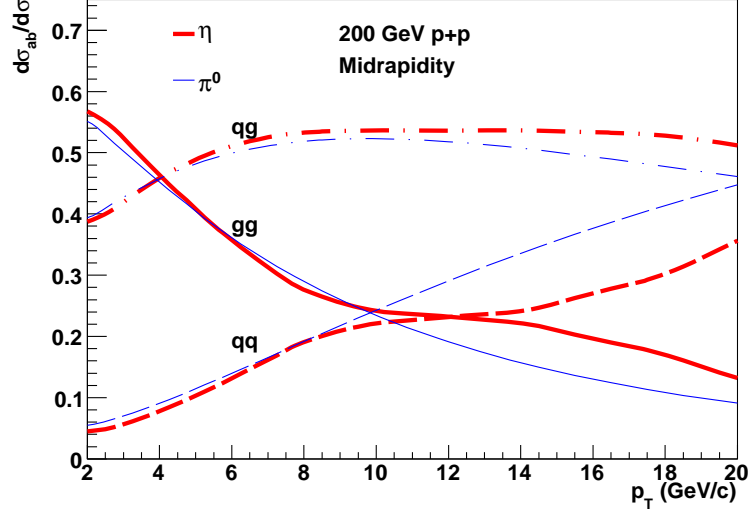


FIG. 4: (color online) Fractional contribution of gluon–gluon (gg), quark–gluon (qg), and quark–quark (qq) scattering to the η production in the pQCD calculation of Fig. 3, and to the π^0 production [24], as a function of p_T .

(qq), to the η production as a function of p_T , are shown in Fig. 4. For comparison, they are also shown in the case of π^0 production [24]. While the corresponding uncertainties are difficult to quantify, it is clear that the subprocess contributions to the η and π^0 production are, within uncertainties, identical up to a p_T of approximately 10 GeV/ c . This is the kinematic range of the η and π^0 double helicity asymmetries presented below and published in Ref. [7, 8], respectively. Consequently, these measurements have approximately the same sensitivity to the gluon helicity distribution accessible via the gg and qg subprocesses. The differences at larger values of p_T are mostly related to uncertainties in the fragmentation functions and thus do not necessarily indicate different sensitivities to polarized PDFs.

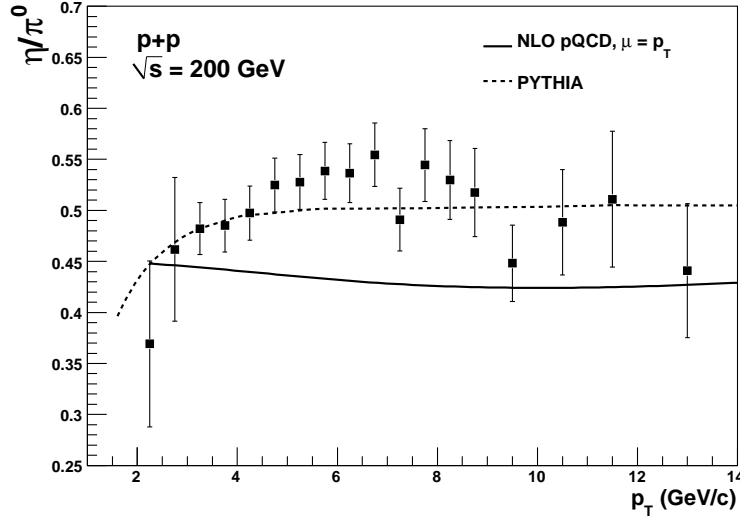


FIG. 5: Cross section ratio for the midrapidity production of inclusive η to π^0 mesons at $\sqrt{s} = 200$ GeV as a function of p_T . The error bars show the statistical and systematic uncertainties added in quadrature. The solid curve shows the ratio of the NLO pQCD calculations shown in Fig. 4 and the corresponding one for the π^0 . The dashed curve shows the result of a PYTHIA Monte-Carlo simulation. See text for details.

Constraining the fragmentation function further should be possible by including precise η to π^0 cross section ratios

in the extraction. The cross section ratio, as a function of p_T , is given in Fig. 5 and Table II. The ratio has been extracted in a single pass over the same data set, thus minimizing systematic uncertainties. In particular, the large normalization uncertainty of 9.7% arising from the luminosity calculation cancels completely. Also all other systematic uncertainties are assumed to either cancel or be reduced to a negligible amount with the exception of the following. The systematic uncertainties due to the η and π^0 peak extraction (type- B_1) and due to the correction for possible merging of the two π^0 decay photons into a single cluster (type- B_2) do not cancel. Furthermore, while the uncertainties on the high- p_T trigger efficiency (type- B_2) are assumed to cancel above $p_T = 4.5$ GeV/ c where the efficiency is flat, a remaining 2% uncertainty on the ratio is assigned for differences in the trigger turn-on curve for $3 < p_T < 4.5$ GeV/ c . Finally, the systematic uncertainty on the acceptance (type- B_2) is reduced to a p_T independent contribution of 2%. The ratio is presented up to $p_T = 14$ GeV/ c only, as beyond this point the statistical and systematic uncertainties become rather large. The latter is due to the fact that for increasing transverse momenta the two photons from the π^0 have a strongly increasing probability of being reconstructed as only a single cluster in the calorimeter, leading to a rather large systematic uncertainty arising from the correction for this effect.

Except for an initial increase due to the different meson masses, the data do not exhibit a strong dependence on p_T . This hints towards a similar dependence of the η and π^0 fragmentation functions on the energy fraction of the parton carried by the hadron. Fitting the cross section ratio, including its statistical and type- B_1 systematic uncertainty, to a constant, gives $R_{\eta/\pi^0} = 0.51 \pm 0.01$ ($\chi^2/\text{ndf} = 18.3/17$), with a remaining systematic uncertainty of 0.01 from the type- B_2 systematic uncertainty. This result does not change when fitting the data above $p_T = 3$ GeV/ c ($\chi^2/\text{ndf} = 14.9/15$) instead of fitting the full range.

Within the uncertainties, the present measurement of η/π^0 is consistent with all previous measurements in $p + p$ collisions, going back to the measurement reported in Ref. [25]. A detailed comparison of subsequent measurements is summarized in Ref. [17]. The observed ratio is in good agreement with a PYTHIA 6.131 [26] calculation [17] shown in the same figure, which is using the default settings and the Lund string fragmentation model [27]. The solid line in Fig. 5 shows the ratio of the NLO pQCD calculations at a scale $\mu = p_T$ (see Fig. 3) and the corresponding one for the π^0 using the same PDF but the π^0 fragmentation function of Ref. [24]. Note that the shape of this calculated cross section ratio is not necessarily well determined as the statistical uncertainty on the η fragmentation function, defined by $\Delta\chi^2 = 2\%$, results in an uncertainty on the η cross section between about 5% and 9%, depending on p_T [18].

The calculated ratio underestimates the data even though the η cross section presented in this paper and earlier PHENIX π^0 data are part of the input in the extraction of the fragmentation functions. This indicates that the constraints from the separate fits are less stringent than fitting the cross section ratio directly. This is obvious from the fact that some of the experimental systematic uncertainties cancel in the ratio as already discussed above, in

TABLE II: Measured η to π^0 cross section ratios vs p_T for the 2006 data set with statistical and systematic (type- B_1 and type- B_2) uncertainties.

p_T (GeV/ c)	η/π^0	stat	type- B_1	type- B_2
2.25	0.369	0.020	0.078	0.007
2.75	0.462	0.024	0.065	0.009
3.25	0.482	0.002	0.022	0.013
3.75	0.485	0.003	0.022	0.014
4.25	0.497	0.004	0.022	0.014
4.75	0.525	0.005	0.023	0.010
5.25	0.528	0.007	0.024	0.011
5.75	0.539	0.009	0.024	0.011
6.25	0.536	0.012	0.024	0.011
6.75	0.555	0.015	0.025	0.011
7.25	0.491	0.019	0.022	0.010
7.75	0.544	0.024	0.024	0.011
8.25	0.530	0.029	0.024	0.011
8.75	0.518	0.035	0.023	0.010
9.5	0.448	0.030	0.020	0.009
10.5	0.488	0.045	0.022	0.014
11.5	0.511	0.058	0.023	0.023
13.0	0.441	0.058	0.020	0.024

particular the overall normalization uncertainty of 9.7% due to the uncertainty in the luminosity measurement. For example, the earlier PHENIX data used in the extraction of the π^0 fragmentation functions was scaled by a factor of 1.09 [24] in the fit, which is within the experimental normalization uncertainty, but leads to a smaller calculated cross section ratio as can be seen in Fig. 5. Also, the dependence of the calculated η and π^0 cross sections on the theoretical scale, as shown in, e.g., Fig. 3, largely cancels in the calculation of the ratio [20]. Hence it appears that improved constraints on η and π^0 fragmentation functions can be derived by directly including the data on the η/π^0 cross section ratio in the fit.

IV. DOUBLE HELICITY ASYMMETRY FOR η MESONS

Experimentally, the double helicity asymmetry (Eq. 1) translates into

$$A_{LL} = \frac{1}{|P_B||P_Y|} \frac{N_{++} - RN_{+-}}{N_{++} + RN_{+-}}, \quad \text{with} \quad R \equiv \frac{L_{++}}{L_{+-}}, \quad (3)$$

where N_{++} (N_{+-}) is the experimental yield for the case where the beams have the same (opposite) helicity. The polarizations of the two colliding beams at RHIC are denoted by P_B and P_Y . The relative luminosity R is measured by a coincident signal in the two BBCs that satisfies the vertex cut. Uncertainties on A_{LL} of 2×10^{-4} (7×10^{-4}) for the 2005 (2006) data due to relative luminosity uncertainties are uncorrelated between years. The asymmetries and uncertainties are combined by weighting by all year-to-year uncorrelated uncertainties in each p_T bin. The results are given in Table III.

The degree of polarization is determined from the combined information of a polarized-proton on carbon ($\vec{p}C$) polarimeter [28], using an unpolarized ultra-thin carbon ribbon target, and from elastic $\vec{p} + \vec{p}$ scattering, using a polarized atomic hydrogen gas-jet target [29]. The average polarization value for the data from 2005 (2006) is 0.49 (0.57). There is a relative uncertainty of 4.8% in the product of the beam polarizations, correlated between the 2005 and 2006 data sets, which is a scale uncertainty on the combined asymmetry result, affecting both the central values and the statistical uncertainties such that the statistical significance of the measurement from zero is preserved. Uncertainties on the products of the beam polarizations that are uncorrelated between years are combined using the same weight factors as for the uncertainties due to relative luminosity, and given in Table III. In order to avoid false asymmetries due to a possible variation of detector response versus time or due to a possible correlation of detector performance with the RHIC bunch structure, all four helicity combinations in the colliding bunches are present within four consecutive bunch crossings. Possible transverse components of the beam polarizations at the PHENIX interaction point are monitored by measuring the spin dependence of very forward neutron production [30] in the zero degree calorimeters [31]. The average transverse component of the product in the 2005 data set is less than 0.014 ± 0.003 , described in more detail in Ref. [7], and was measured to be negligible in the 2006 data set.

Accounting for the asymmetry of the background (BG) under the η peak, the double helicity asymmetry for η production,

$$A_{LL}^{\eta} = \frac{A_{LL}^{\eta+\text{BG}} - r A_{LL}^{\text{BG}}}{1 - r}, \quad \text{with} \quad r \equiv \frac{N^{\text{BG}}}{N^{\eta} + N^{\text{BG}}}, \quad (4)$$

is calculated by separately measuring the asymmetry in the 2σ window around the mean of the η peak ($A_{LL}^{\eta+\text{BG}}$) and (as described above) in the sidebands (A_{LL}^{BG}).

The latter is consistent with zero. The resulting background corrected asymmetry for η production as a function of p_T from the combined 2005 and 2006 data is shown in Fig. 6 and tabulated in Table III. It is consistent with zero over the measured range as can be expected based on the similar contributions of the various scattering subprocesses to the η and π^0 production shown in Fig. 4 and the fact that the double helicity asymmetry for π^0 production [8] is consistent with zero as well.

As can be seen in Fig. 6, the η double helicity asymmetry is in agreement with NLO pQCD calculations using the above mentioned fragmentation functions and two different sets of polarized PDFs[6, 32] as an input to the code of Ref. [23].

These data can be used in global fits in order to further constrain polarized PDFs, in particular the helicity-dependent gluon PDF. In the future, with improved statistics and the availability of flavor-separated fragmentation functions, double-helicity asymmetries in η production can potentially constrain the polarized strange quark PDF (Δs) due to the additional s -quark contribution in the η wave function. Special interest in Δs arises from the fact that its value is negative, when extracted from analyses of inclusive DIS data, using hyperon decay data and assuming SU(3) flavor symmetry [2, 3], but consistent with zero, when directly extracted from semi-inclusive DIS data [33–35]. Global fits can constrain PDFs by simultaneously describing a wide variety of experimental channels over a

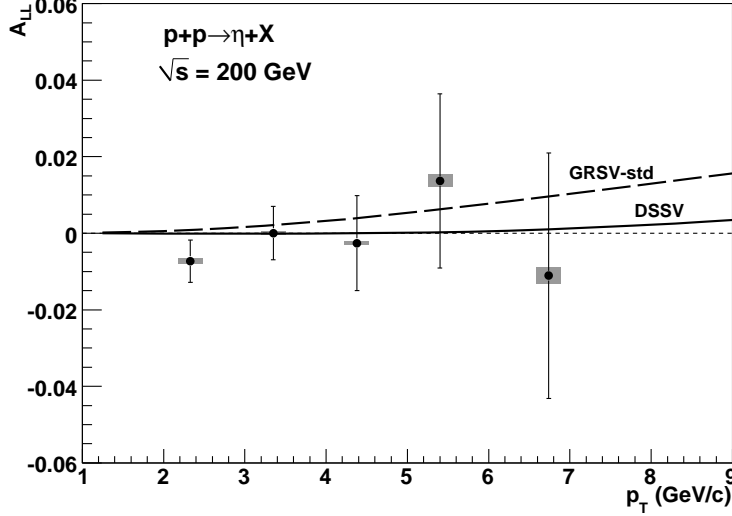


FIG. 6: Double helicity asymmetry for midrapidity inclusive η production from the combined 2005 and 2006 data at $\sqrt{s} = 200$ GeV as a function of p_T . The gray boxes are point-to-point systematic uncertainties due to polarization and relative luminosity uncertainties and are correlated point-to-point, moving all points in the same direction but not by the same factor. An additional systematic uncertainty of 4.8% on the vertical scale due to the uncertainty in the beam polarizations is not shown. The results are compared to NLO pQCD calculations using two different sets of polarized PDFs[6, 32]. See text for details.

TABLE III: Double-helicity asymmetry values and uncertainties vs $\langle p_T \rangle$ for the combined 2005 and 2006 data sets. Systematic uncertainties given are type B_2 , scaling all points in the same direction but not by the same factor, and are due to polarization (σ_{syst}^P) and relative luminosity (σ_{syst}^R) uncertainties that are uncorrelated between years. There is an additional type C systematic uncertainty of 4.8% on the vertical scale due to uncertainty in the beam polarizations that is correlated between years.

$\langle p_T \rangle$ (GeV/c)	A_{LL}	σ_{stat}	σ_{syst}^P	σ_{syst}^R
2.33	-0.0073	0.0055	0.0006	0.0004
3.35	0.0000	0.0070	0.0000	0.0004
4.38	-0.0026	0.0124	0.0002	0.0004
5.40	0.0137	0.0228	0.0016	0.0004
6.74	-0.0111	0.0320	0.0021	0.0004

range of kinematics with different sensitivities, different experimental systematic uncertainties, and different sources of theoretical uncertainty. Thus, the data presented here open up a valuable new channel to improve knowledge of polarized PDFs.

V. SUMMARY

The double helicity asymmetry in η production is measured and found to be consistent with zero in the transverse momentum range between 2 GeV/c and 9 GeV/c. The η cross section is determined over seven orders of magnitude between 2 GeV/c and 20 GeV/c in transverse momentum. In particular due to the wide range in transverse momentum these data serve as important input for the extraction of fragmentation functions. The η to π^0 cross section ratio as a function of p_T has been extracted in a single pass over the same data set, thus minimizing systematic uncertainties. A fit to a constant above $p_T = 2$ GeV/c or $p_T = 3$ GeV/c yields a value of $R_{\eta/\pi^0} = 0.51 \pm 0.01^{\text{stat}} \pm 0.01^{\text{syst}}$. The inclusion of these data on the ratio in future fragmentation function extractions should allow for more precise results for both particle species. This opens up the possibility to include the data on the double helicity asymmetry in future NLO pQCD fits in order to further constrain the polarized parton distribution functions, in particular the helicity-dependent gluon distribution function.

Acknowledgments

We thank the staff of the Collider-Accelerator and Physics Departments at Brookhaven National Laboratory and the staff of the other PHENIX participating institutions for their vital contributions. We also thank M. Stratmann and R. Sassot for fruitful discussions. We acknowledge support from the Office of Nuclear Physics in the Office of Science of the Department of Energy, the National Science Foundation, a sponsored research grant from Renaissance Technologies LLC, Abilene Christian University Research Council, Research Foundation of SUNY, and Dean of the College of Arts and Sciences, Vanderbilt University (USA), Ministry of Education, Culture, Sports, Science, and Technology and the Japan Society for the Promotion of Science (Japan), Conselho Nacional de Desenvolvimento Científico e Tecnológico and Fundação de Amparo à Pesquisa do Estado de São Paulo (Brazil), Natural Science Foundation of China (People's Republic of China), Ministry of Education, Youth and Sports (Czech Republic), Centre National de la Recherche Scientifique, Commissariat à l'Énergie Atomique, and Institut National de Physique Nucléaire et de Physique des Particules (France), Ministry of Industry, Science and Technologies, Bundesministerium für Bildung und Forschung, Deutscher Akademischer Austausch Dienst, and Alexander von Humboldt Stiftung (Germany), Hungarian National Science Fund, OTKA (Hungary), Department of Atomic Energy (India), Israel Science Foundation (Israel), National Research Foundation and WCU program of the Ministry Education Science and Technology (Korea), Ministry of Education and Science, Russia Academy of Sciences, Federal Agency of Atomic Energy (Russia), VR and the Wallenberg Foundation (Sweden), the U.S. Civilian Research and Development Foundation for the Independent States of the Former Soviet Union, the US-Hungarian Fulbright Foundation for Educational Exchange, and the US-Israel Binational Science Foundation.

-
- [1] J. Blumlein and H. Bottcher, Nucl. Phys. **B841**, 205 (2010).
 - [2] A. Airapetian et al. (HERMES Collaboration), Phys. Rev. D **75**, 012007 (2007).
 - [3] V. Y. Alexakhin et al. (COMPASS Collaboration), Phys. Lett. **B647**, 8 (2007).
 - [4] M. Alekseev et al. (COMPASS Collaboration), Phys. Lett. **B676**, 31 (2009).
 - [5] A. Airapetian et al. (HERMES Collaboration), JHEP **08**, 130 (2010).
 - [6] D. de Florian, R. Sassot, M. Stratmann, and W. Vogelsang, Phys. Rev. Lett. **101**, 072001 (2008).
 - [7] A. Adare et al. (PHENIX Collaboration), Phys. Rev. D **76**, 051106 (2007).
 - [8] A. Adare et al. (PHENIX Collaboration), Phys. Rev. Lett. **103**, 012003 (2009).
 - [9] A. Adare et al. (PHENIX Collaboration), Phys. Rev. D **79**, 012003 (2009).
 - [10] B. I. Abelev et al. (STAR Collaboration), Phys. Rev. Lett. **100**, 232003 (2008).
 - [11] C. Amsler et al. (Particle Data Group), Phys. Lett. **B667**, 1 (2008).
 - [12] K. Adcox et al. (PHENIX Collaboration), Nucl. Instrum. Meth. **A499**, 469 (2003).
 - [13] M. Allen et al. (PHENIX Collaboration), Nucl. Instrum. Meth. **A499**, 549 (2003).
 - [14] L. Aphecetche et al. (PHENIX Collaboration), Nucl. Instrum. Meth. **A499**, 521 (2003).
 - [15] S. S. Adler et al. (PHENIX Collaboration), Phys. Rev. Lett. **91**, 241803 (2003).
 - [16] G. D. Lafferty and T. R. Wyatt, Nucl. Instrum. Meth. **A355**, 541 (1995).
 - [17] S. S. Adler et al. (PHENIX Collaboration), Phys. Rev. C **75**, 024909 (2007).
 - [18] C. A. Aidala, F. Ellinghaus, R. Sassot, J. P. Seele, and M. Stratmann (2010), arXiv:1009.6145 [hep-ph].
 - [19] D. Indumathi, H. S. Mani, and A. Rastogi, Phys. Rev. D **58**, 094014 (1998).
 - [20] D. Indumathi and B. Misra (2008), arXiv:0901.0228 [hep-ph].
 - [21] M. Greco and S. Rolli, Z. Phys. **C60**, 169 (1993).
 - [22] J. Pumplin et al., JHEP **07**, 012 (2002).
 - [23] B. Jäger, A. Schäfer, M. Stratmann, and W. Vogelsang, Phys. Rev. D **67**, 054005 (2003).
 - [24] D. de Florian, R. Sassot, and M. Stratmann, Phys. Rev. D **75**, 114010 (2007).
 - [25] F. W. Busser et al., Phys. Lett. **B55**, 232 (1975).
 - [26] T. Sjöstrand et al., Comput. Phys. Commun. **135**, 238 (2001).
 - [27] B. Andersson, G. Gustafson, G. Ingelman, and T. Sjöstrand, Phys. Rept. **97**, 31 (1983).
 - [28] I. Nakagawa et al., AIP Conf. Proc. **980**, 380 (2008).
 - [29] H. Okada et al., Phys. Lett. **B638**, 450 (2006).
 - [30] A. Bazilevsky et al., Phys. Lett. **B650**, 325 (2007).
 - [31] C. Adler et al., Nucl. Instrum. Meth. **A470**, 488 (2001).
 - [32] M. Glück, E. Reya, M. Stratmann, and W. Vogelsang, Phys. Rev. D **63**, 094005 (2001).
 - [33] A. Airapetian et al. (HERMES Collaboration), Phys. Rev. D **71**, 012003 (2005).
 - [34] A. Airapetian et al. (HERMES Collaboration), Phys. Lett. **B666**, 446 (2008).
 - [35] M. G. Alekseev et al. (COMPASS Collaboration) (2010), 1007.4061.